




Designing and fabrication of a novel gold nanocomposite structure: application in electrochemical sensing of bisphenol A

Mehdi Baghayeri, Reza Ansari, Marzieh Nodehi & Hojat Veisi

To cite this article: Mehdi Baghayeri, Reza Ansari, Marzieh Nodehi & Hojat Veisi (2018) Designing and fabrication of a novel gold nanocomposite structure: application in electrochemical sensing of bisphenol A, International Journal of Environmental Analytical Chemistry, 98:9, 874-888, DOI: 10.1080/03067319.2018.1512595

To link to this article: <https://doi.org/10.1080/03067319.2018.1512595>

 View supplementary material 

 Published online: 16 Sep 2018.

 Submit your article to this journal 


 Article views: 8

 View Crossmark data 

ARTICLE



Designing and fabrication of a novel gold nanocomposite structure: application in electrochemical sensing of bisphenol A

Mehdi Baghayeri ^a, Reza Ansari^b, Marzieh Nodehi^b and Hojat Veisi^c

^aDepartment of Chemistry, Faculty of Science, Hakim Sabzevari University, Sabzevar, Iran; ^bDepartment of Chemistry, Faculty of Science, University of Guilan, Rasht, Iran; ^cDepartment of Chemistry, Payame Noor University, Tehran, Iran

ABSTRACT

In this article, a highly sensitive electrochemical sensor is introduced for direct electro-oxidation of bisphenol A (BPA). The novel nanocomposite was prepared based on multi-walled carbon nanotube/thiol functionalised magnetic nanoparticles ($\text{Fe}_3\text{O}_4\text{-SH}$) as an immobilisation platform and gold nanoparticles (AuNPs) as an amplifying electrochemical signal. The chemisorbed AuNPs exhibited excellent electrochemical activity for the detection of BPA. Some analysing techniques such as Fourier transform infrared spectroscopy, field emission scanning electron microscopy, transmission electron microscopy and energy-dispersive x-ray diffraction exposed the formation of nanocomposite. Under optimum conditions (pH 9), the sensor showed a linear range between 0.002–240 μM , with high sensitivity ($0.25 \mu\text{A} \mu\text{M}^{-1}$) along with low detection limit ($6.73 \times 10^{-10} \text{ M}$). Moreover, nanocomposites could efficiently decrease the effect of interfering agents and remarkably enhance the utility of sensor at detection of BPA in some real samples.

ARTICLE HISTORY

Received 19 March 2018
Accepted 8 August 2018

KEYWORDS

Gold nanoparticle; bisphenol A; electrochemical behaviour; immobilisation platform; sensors

1. Introduction

Production and consumption of plastics has grown globally from 1950. Today, China and North America are the largest producers of plastics materials worldwide. Plastics meet the needs of a wide variety of markets. European plastics demand shows that 39.5% of plastics were used at packing industry in 2014 [1]. Studies proved that 2,2-bis(4-hydroxyphenyl)propane, so-called bisphenol A (BPA), is a main agent for manufacture of plastics. BPA can permeate into food and drinking water from a wide variety of food container materials mainly derived from polycarbonates, epoxy resins, and unsaturated polyesters [2]. Food and drink containers, milk bottles, papers, packing materials and engineering plastics can act as carriers of this organic contaminant in food and environment. Estrogenicity of BPA *in vitro* is similar to the 17β -estradiol which can mimic hormones and disrupt endocrine function. Therefore, BPA displays an adverse effect in human immune function and has been related to heart diseases, elevation of levels of

CONTACT Mehdi Baghayeri  m.baghayeri@hsu.ac.ir
 Supplemental data for this article can be accessed [here](#)

© 2018 Informa UK Limited, trading as Taylor & Francis Group

some serum liver enzymes and cancers of the mammary gland and prostate gland [3–8]. Therefore, it is quite logical that detection of BPA in various analytical methods such as liquid chromatography-mass spectrometry [9], gas chromatography coupled with mass spectrometry [10], capillary electrophoresis [11], electrochemiluminescence detection [12] and fluorimetry [13] is an interesting field of research. But the challenge of these techniques lies in expensive testing equipment, complicated sample pretreatment and not being competent for on-site detection in emergent pollution events [14]. In fact, it is urgently necessary to develop high-selectivity and high-sensitivity sensors for on-site detection of BPA. For fabrication of an ideal sensor, first, a detection agent with high affinity and specificity is helpful to determine the analyte (here BPA) and, second, a sensitive detection system needs features such as real-time readout ability. In this way, a simple investigation reveals that the electrochemical BPA sensors were regarded as one of the acceptable and extensible methods among other analytical approaches. For example, Beitollahi et al. reported construction of a nanostructure-based electrochemical sensor for voltammetric determination of BPA with a detection limit of 55.0 nM [15]. Zhan et al. developed an electrochemical BPA sensor based on exfoliated Ni₂Al-layered double hydroxide nanosheet modified electrode [16]. Tan et al. prepared a highly sensitive molecularly imprinted polypyrrole/graphene quantum dots composite for detection of BPA in water samples [17].

In electrochemical sensing methods, much attention has been focused on selection of appropriate modifiers due to their potential abilities for reduction of overpotential and/or increase of current for analyte detection. Carbon-based nanostructures as excellent heterogeneous platforms have attracted much attention for the modification of electrode surfaces. Their proven properties such as uniform nanostructure, electrical conductivity, high specific surface area and appropriate chemical stability make them proper candidates for corroboration at modification process. However, sensors based on CNTs suffer from poor sensing factors such as lack of selectivity, irreversibility and slow response time. The key solution to this problem is functionalisation of CNT sidewalls with specific compounds such as magnetic nanoparticles (MNPs), metal oxides and noble metal nanoparticles [18,19].

MNPs have recently received significant attention for fabrication of sensing devices. The favourable properties of MNPs such as chemical inertness, magnetic properties, no toxicity and thermal stability allow MNPs to be simply functionalised by organic or inorganic groups. Karaoglu et al. reported synthesis and characteristics of poly(3-pyrrol-1-ylpropanoic acid)-Fe₃O₄ nanocomposite via *in situ* polymerisation of 1-(2-carboxyethyl) pyrrole in the presence of Fe₃O₄ nanoparticles [20]. Mai et al. demonstrated that the interaction between red blood cells and carboxylated core-shell magnetic nanoparticles is mainly ruled by electrostatic attraction [21]. Gao et al. investigated fabrication of molecularly imprinted polymers by amino-modified Fe₃O₄ nanoparticles for unique detection of bovine haemoglobin [22]. In recent years, our research team reported fabrication of electrochemical biosensors based on iron oxide MNPs, functionalised with different polymers and copolymers [23–26]. The objective of our investigation was to study the interaction of functionalised iron oxide MNPs with proteins and enzymes. On the other hand, the selection of efficient chemical compound with special functional groups immobilised on MNPs can provide an opportunity to modify them with other heterogeneous nanomaterials and increase

their operational performance in various applications. At such structures, noble metals with high catalytic activity and high surface area can act as a key signal receiver enhancing electrochemical signal of analytes [27]. Peng et al. reported synthesis of efficient polydopamine-Fe₃O₄ MNPs for immobilisation of Au nanoparticles and used it for detection of hydrogen peroxide [28]. Han et al. used the Fe₃O₄ NPs functionalised with glutathione and gold nanoparticles (AuNPs) for detection of estradiol [29]. Integration of the multi-walled carbon nanotubes (MWCNTs), AuNPs and Fe₃O₄NPs can provide a unique sensing platform with strong synergistic effects for electro-oxidation of BPA. MWCNTs provide sufficient substrates for Fe₃O₄NPs immobilisation. MNP prevents the accumulation of AuNPs, and the AuNPs accelerate electron transfer on the surface of electrode with their catalytic property.

The objective of this study was to develop a sensitive and selective electrochemical method for detection and determination of BPA. Therefore, a novel MNP-supported triethoxypropylthiole gold nanocomposite was successfully prepared by attaching AuNPs to thiol-functionalised Fe₃O₄ nanoparticles (Fe₃O₄-SH/Au). The as-prepared nanocomposite was well attached to MWCNTs (MWCNTs/Fe₃O₄-SH/Au) and was applied in fabrication of an electrochemical sensor after casting on a glassy carbon (GC) electrode (GCE/MWCNTs/Fe₃O₄-SH/Au). It was found that the synthesised nanocomposite be highly efficient for the electro-oxidation of BPA.

2. Experimental

2.1. Reagents and apparatus

BPA was supplied from Merck chemical company (www.merckmillipore.com, Germany). Triethoxypropylthiole, sodium borohydride, MWCNTs (>95%, O.D.: 10–15 nm, I.D.: 2–6 nm, length: 0.1–10 μm) and chloroauric acid trihydrate (HAuCl₄·3H₂O) were all obtained from Sigma-Aldrich (www.sigmaaldrich.com, USA) and used without further purification. Phosphate buffer solution (PBS, 0.1 M, pH 9) was prepared by mixing solutions of 0.2 M Na₂HPO₄ · 12H₂O and 0.2 M NaH₂PO₄·H₂O. The stock solutions of BPA (0.01 M) were prepared in minimum ethanol and PBS (pH 9). All the solutions were prepared using double-distilled water.

All electrochemical experiments were done on a PalmSens Instrumentation (Palm Instrument BV, the Netherlands) in the electrochemical cell consisting of a GC, modified or unmodified, as working electrode (3 mm diameter, Azar electrode, Iran); a platinum wire, as counterelectrode; and a Ag|AgCl|KCl (3M), as reference electrode. Cyclic voltammetric measurements were carried out over a potential range from 0.0 to 1.0 V with a scan rate of 0.1 V s⁻¹. Electrochemical impedance spectroscopy was performed in 5.0 mM K₃Fe(CN)₆/K₄Fe(CN)₆ (1/1) mixture with 0.1 M KCl as the supporting electrolyte, using an applied potential of 0.2 V, amplitude of 10 mV and a frequency range of 0.1–50,000 Hz. The differential pulse voltammograms (DPVs) were obtained under the following conditions: the voltage scanned from +0.3 to +0.7 V with a pulse height of 50 mV, and the step height and the pulse time were kept as 10 mV and 0.2 S, respectively. The morphology and structure of nanoparticles were investigated by field emission scanning electron microscopy (FESEM) (Hitachi S4160 instrument, Tokyo, Japan) and a Hitachi HT-7100 (150 kV) transmission electron microscope (TEM). Fourier

transform infrared (FT-IR) spectra were recorded on a Perkin Elmer GX FT-IR spectrometer. All experiments were performed at room temperature ($25 \pm 2^\circ\text{C}$).

The synthesis process and characterisation of MWCNTs/Fe₃O₄-SH/Au nanocomposite is described in the Supplementary material.

2.2. Preparation of modified electrode

After obtaining a mirror-like surface from polished GC electrode, it was rinsed separately with ethanol and double-distilled water by sound waves for 2 min and allowed to dry at room temperature. In the next step, 5 μL of MWCNTs/Fe₃O₄-SH/Au nanocomposite, dispersed at ethanol 0.1% (W/V), was casted on to GCE to fabricate the GCE/MWCNTs/Fe₃O₄-SH/Au after drying at room temperature. For comparison purposes, MWCNTs/Fe₃O₄-SH modified GC electrode was also prepared according to the same procedure and named as GCE/MWCNTs/Fe₃O₄-SH.

3. Results and discussion

3.1 Characterisation of MWCNTs/Fe₃O₄-SH/Au nanocomposite

FT-IR characterisation for Fe₃O₄ (Figure 1(a)), Fe₃O₄-SH (Figure 1(b)), Fe₃O₄-SH/Au (Figure 1(c)), MWCNTs-NH₂ (Figure 1(d)) and MWCNTs/Fe₃O₄-SH/Au nanocomposite (Figure 1(e)) was performed. In the FT-IR spectrum of Fe₃O₄ NPs, the bands around 3408, 1625 and 637 cm^{-1} attributed to the O-H stretching vibration, H-O-H bending vibration and Fe-O stretching vibration, respectively. In FT-IR of Fe₃O₄-SH, peaks at 1449 and 2928 cm^{-1} appeared that related to aliphatic bending vibrations and stretching vibrations of CH₂ groups in mercaptopropyl groups. Also, a new peak was at 2361 cm^{-1} corresponding to the mercaptans stretching (-SH) in mercaptopropyl groups and two new peaks were at 1127 and 1037 cm^{-1} which may be related to the Fe-O-Si bonds [30]. Moreover, stretching and bending vibrations of Fe₃O₄NPs are seen in the FT-IR spectrum of Fe₃O₄ NPs, which confirms the functionalisation of Fe₃O₄NPs. In the FT-IR spectrum of Fe₃O₄-SH/Au, a weak peak at 2361 cm^{-1} is eliminated, which can be related to interaction between -SH groups with AuNPs. In curve 1d, the presence of peaks at 3447 and 1741 cm^{-1} is related to the stretching vibrations of $\nu(\text{OH})$ and $\nu(\text{C}=\text{O})$ of the carboxyl groups (COOH) in the MWCNTs-NH₂. Symmetric and asymmetric vibrations of CH₂ groups at 2868 and 2923 cm^{-1} , respectively, are observed in MWCNTs-NH₂. It is assumed that defective sites on the sidewall of MWCNTs contain these groups. Stretching vibrations of the amine group (-NH₂) overlap with the stretching vibration of $\nu(-\text{OH})$ in the MWCNTs-NH₂. In Figure 1(e), it can be seen that the absorption bands Fe₃O₄-SH/Au and MWCNTs exist; also, the absorption band around 3408 cm^{-1} decreased, which is the evidence of the interaction between MWCNTs and functionalised Fe₃O₄ nanoparticles. These absorption bands represent that the synthesis of MWCNTs/Fe₃O₄-SH/Au nanocomposite was successful.

Characterisation of the surface morphology of MWCNTs/Fe₃O₄-SH/Au nanocomposite was studied through FESEM and TEM. Figure 2(a) shows the representative FESEM image of as-synthesised nanocomposite. In an overview, it can be seen that the surface of MWCNTs/Fe₃O₄-SH/Au nanocomposite is rough and porous. Actually, the effective surface area and efficient sites can significantly increase at such structures and help to

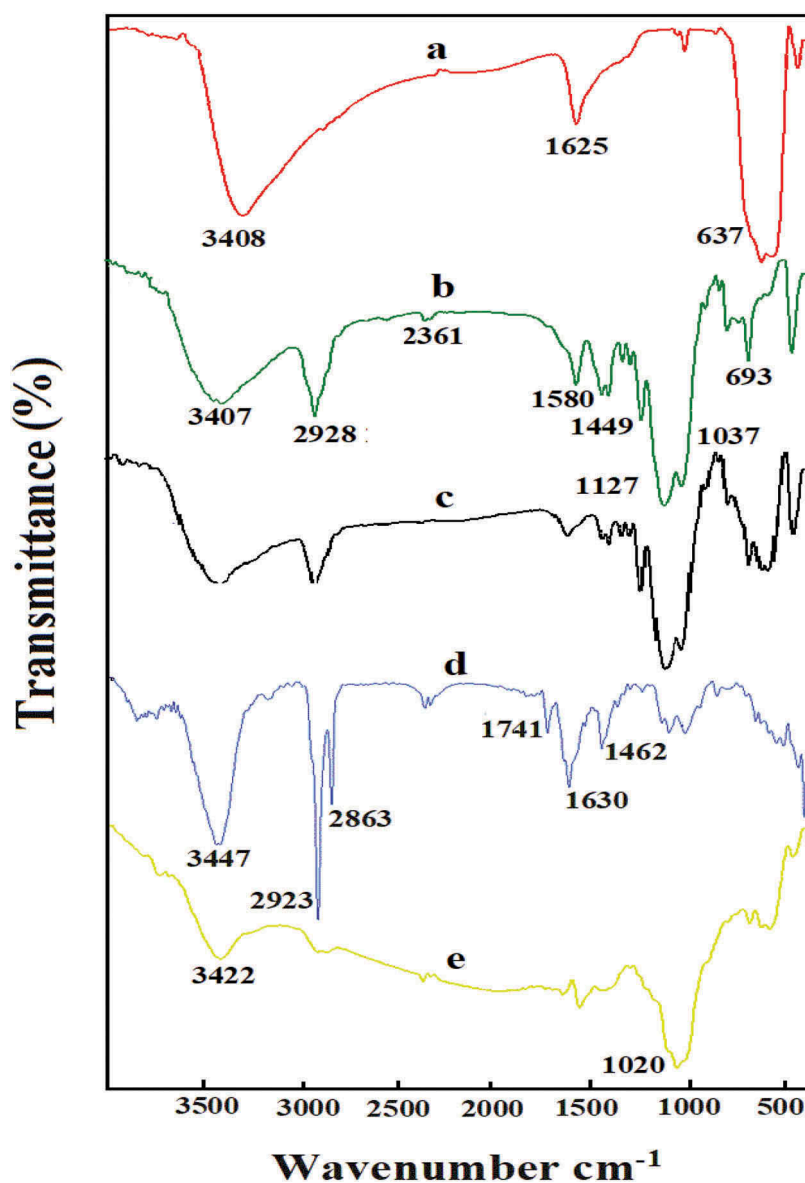


Figure 1. FT-IR spectra of Fe_3O_4 (a), $\text{Fe}_3\text{O}_4\text{-SH}$ (b), $\text{Fe}_3\text{O}_4\text{-SH/Au}$ (c), MWCNTs- NH_2 (d) and MWCNTs/ $\text{Fe}_3\text{O}_4\text{-SH/Au}$ nanocomposite (e).

improve the electrochemical signal and decrease the detection limit. Moreover, the distribution of AuNPs and Fe_3O_4 NPs was also observable in MWCNTs with a size distribution of 30–60 nm (see inset image of Figure 2(a)). The corresponding EDX patterns for the $\text{Fe}_3\text{O}_4\text{-SH/Au}$ deposited on the MWCNTs surface are shown in Figure 2 (b). From these results, we can conclude that the MWCNTs uniformly covered Fe_3O_4 and Au nanoparticles. TEM measurements were performed to further confirm the presence of Fe_3O_4 and Au nanoparticles on the MWCNTs at the structure of nanocomposite. The TEM image of $\text{Fe}_3\text{O}_4\text{-SH/Au}$ nanocomposite (Figure 2(c)) demonstrates that Au seeds

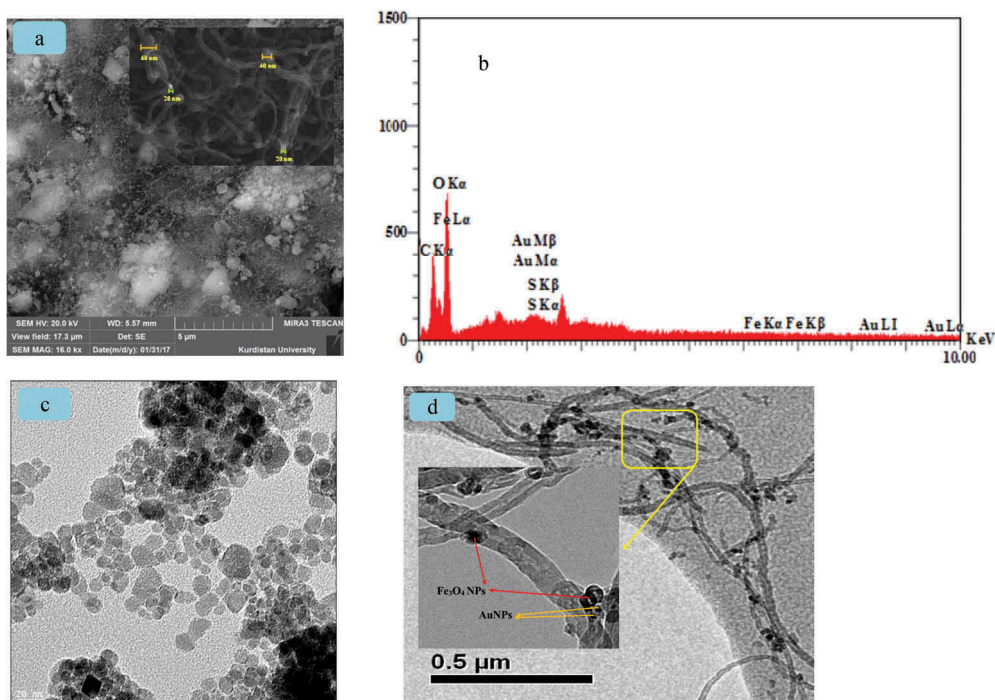


Figure 2. (a) The FESEM image of MWCNTs/Fe₃O₄-SH/Au nanocomposite. Inset: the FESEM image of MWCNTs/Fe₃O₄-SH/Au nanocomposite with a detailed observation. (b) EDX pattern of MWCNTs/Fe₃O₄-SH/Au nanocomposite. (c) TEM images of Fe₃O₄-SH/Au nanocomposite. (d) TEM images of MWCNT/Fe₃O₄-SH/Au nanocomposite.

decorated on the magnetic Fe₃O₄ nanoparticles. Figure 2(d) shows a representative TEM image of MWCNTs coated with Fe₃O₄ and Au nanoparticles. With a detailed observation (Figure 2(d), down right), it clearly reveals that the NPs have been distributed on the surface of CNTs.

Electrochemical properties of nanocomposite were performed in order to investigate the existence of AuNPs in nanocomposites. The results are listed in Supplementary material.

3.2 Electrochemical characterisation of MWCNTs/Fe₃O₄-SH/Au nanocomposite modified GCE

The redox couple [Fe(CN)₆]^{4-/3-}, as the electrochemical probe, was applied to electrochemical study of the different modified electrodes. Figure S2 shows the cyclic voltammograms recorded for the bare GCE (curve a), GCE/MWCNTs (curve b), GCE/MWCNTs/Fe₃O₄-SH (curve c) and GCE/MWCNTs/Fe₃O₄-SH/Au (curve d) for a 5 mM K₄Fe(CN)₆ in 0.1 M KCl solution. Table S1 presents the calculated important electrochemical values of ΔE_p, anodic (j_a) and cathodic (j_c) current densities, and electroactive area (A) for each modified electrode. The ΔE_p provides information regarding the electron transfer kinetics through the electrode surface. A faster electron transfer is revealed by lower ΔE_p value for the redox probe at the electrode surface. Investigation of ΔE_p values for the different electrodes exhibits that the [Fe(CN)₆]^{4-/3-} has a lower ΔE_p (125 mV) on the

GCE/MWCNTs/Fe₃O₄-SH/Au. This confirms that the presence of AuNPs at the nanocomposite structure provides a better electron transfer. The obtained peak current is an important parameter for electroanalytical purposes that can be obtained by characterisation of different electrodes with redox probe. An evaluation of the j_a and j_c achieved for different modified electrodes (Table S1) shows that these currents are higher for the MWCNTs/Fe₃O₄-SH/Au nanocomposites.

On the other hand, according to Randles–Sevcik equation (Equation 1), the electroactive surface area for each electrode can be calculated from registration of current changes vs. different scan rates [31]:

$$I_p = (2.69 \times 10^5) An^{3/2} D^{1/2} C_0 \nu^{1/2} \quad (1)$$

In this equation, I_p is the anodic or cathodic peak current, n is the number of transferred electrons for the redox reaction, A is the effective surface area (cm²), D and C_0 are the diffusion coefficient and bulk concentration of the redox probe, and ν is the potential scan rate (V s⁻¹). In accordance with the above discussion, cyclic voltammetry experiments were carried out at different scan rate from 0.025 to 0.300 V s⁻¹. As listed in Table S1, the electroactive surface area for studied electrodes increased in the following order: GCE < GCE/MWCNTs < GCE/MWCNTs/Fe₃O₄-SH < GCE/MWCNTs/Fe₃O₄-SH/Au. However, the electrodes that contain higher electroactive surface area will be more effective in electroanalytical applications [32].

The operation of as-prepared modified electrodes was evaluated by Nyquist impedance plots. The Nyquist plots of GCE/MWCNTs/Fe₃O₄-SH/Au, GCE/MWCNTs/Fe₃O₄-SH, GCE/MWCNTs and GCE over a frequency range from 0.1 to 50,000 Hz, as shown in Figure S3. The typical Nyquist plot can be divided into three different regions base of the change at frequency range. The intersection point on the real axis (Z'), at high frequency, corresponds to the internal resistance of the electrode and the ohmic resistance of the electrolyte (R_s). At high to middle frequency, the semicircular plot represents the charge transfer resistance (R_{ct}). Also, the diffusion of redox probe ions to the inside electrode provides the transition from the semicircle to the long tail at low frequency [33]. Based on the obtained plot in the high-frequency range, the R_s and R_{ct} are 84.3 and 912.7 Ω for GCE/MWCNTs/Fe₃O₄-SH/Au, 97.8 Ω and 1406.2 Ω for GCE/MWCNTs/Fe₃O₄-SH, 85.9 Ω and 1675.8 Ω for GCE/MWCNTs and 130.0 Ω and 1976.0 Ω for GCE, respectively. The R_s of GCE/MWCNTs/Fe₃O₄-SH/Au and GCE/MWCNTs/Fe₃O₄-SH are lower than that of GCE, suggesting that the improved electric conductivity of the modified electrodes is because of the presence of MWCNTs/Fe₃O₄-SH and AuNPs. As expected, the R_{ct} of GCE/MWCNTs/Fe₃O₄-SH/Au is slightly lower than that of GCE/MWCNTs/Fe₃O₄-SH, which can be explained by better accessibility and low charge transfer resistance of nanocomposite due to distributed AuNPs on functionalised carbon nanotube surface.

3.3 The electro-catalytic oxidation of bisphenol A

Cyclic voltammograms of different electrodes in absence and presence of BPA are shown in Figure 3. An irreversible oxidation peak can be seen on the cyclic voltammograms, which was corresponding to the oxidation of BPA. However, the potential and oxidation peak current exhibited various values at different electrodes, which proved the effect of

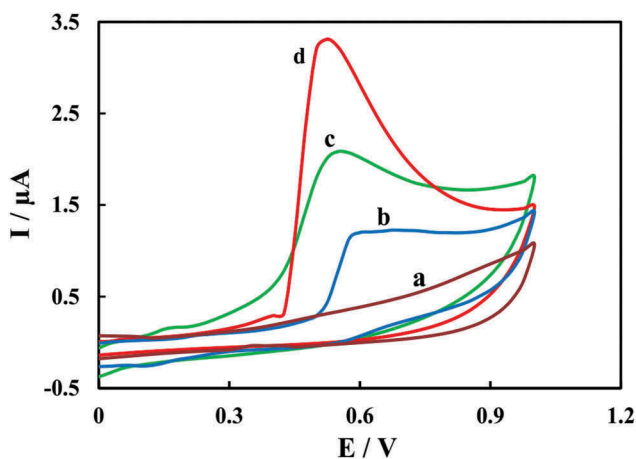


Figure 3. Cyclic voltammograms of 0.1 mM BPA in 0.1 M PBS at the surface of different electrodes: bare GCE (b), GCE/MWCNTs/Fe₃O₄-SH (c) and GCE/MWCNTs/Fe₃O₄-SH/Au (d) at scan rate of 0.1 V s⁻¹. Curve a shows the cyclic voltammogram of the GCE/MWCNTs/Fe₃O₄-SH/Au in absence of BPA.

the modifier on the electrode surface. Compared with that of GCE (curve b), the oxidation peak current increased with the negative shift of the oxidation peak potential on the GCE/MWCNTs/Fe₃O₄-SH (curve c) and GCE/MWCNTs/Fe₃O₄-SH/Au (curve d), which indicated the effect of MWCNTs/Fe₃O₄-SH and MWCNTs/Fe₃O₄-SH/Au on electrooxidation of BPA. In the case of GCE/MWCNTs/Fe₃O₄-SH, the presence of MWCNTs and Fe₃O₄-SH on the electrode surface acts as a catalyst in the electro-oxidation process. On the other hand, in GCE/MWCNTs/Fe₃O₄-SH/Au, the anodic peak current grew more with the further negative shift of the oxidation peak potential, representing that the intrinsic conductivity of immobilised AuNPs on the surface of electrode could significantly increase the electron transfer rate. Actually, AuNPs have increased the electron transfer rate between the electrode surface and analyte. On the other hand, the presence of AuNPs increased the absorption of the analyte on the surface of the electrode, which improved the sensitivity of the electrode for BPA detection. Furthermore, the porous structure of MWCNTs/Fe₃O₄-SH/Au nanocomposite has reinforced the mass and electron transport of electrolytes at the electrode-electrolyte interface. So the synthesised nanocomposite is a favourable choice for the construction of BPA electrochemical sensor.

The electrochemical response of GCE/MWCNTs/Fe₃O₄-SH/Au on electro-oxidation of BPA was further studied via changing the scan rate in the range from 0.025 to 0.3 V s⁻¹. As it can be seen from Figure 4(A), with the increase of potential scan rate, oxidation peak current of BPA increased gradually proportional to the scan rate with the linear regression equation as $I_p(\mu\text{A}) = 14.563 v (\text{V s}^{-1}) + 0.8805$ ($R^2 = 0.9924$). The results showed that the electrochemical reaction was a surface-controlled adsorption process. In order to get the information about the rate determining step, a Tafel plot was drawn using the data derived from the rising part of the current-voltage curve recorded at a scan rate of 0.075 V s⁻¹. (Figure 4(B)). This part of voltammogram is affected by electron transfer kinetics of analyte (here BPA) and electrode surface. With assumption of a two-electron transfer process and with the help of calculated slope from Tafel region of 13.85 V decade⁻¹, a charge transfer coefficient of $\alpha = 0.43$ was

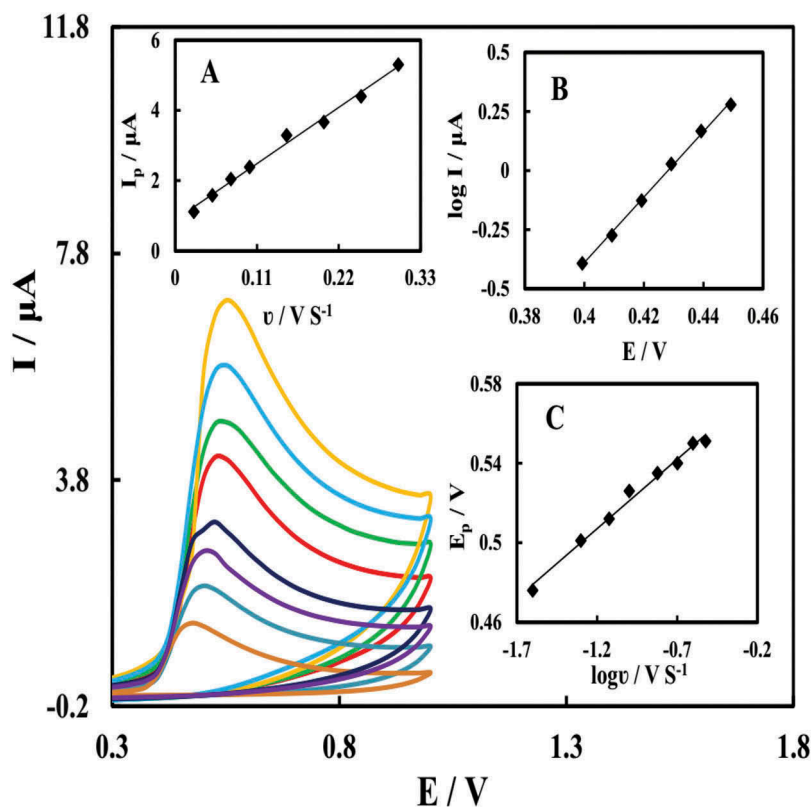


Figure 4. Cyclic voltammograms of GCE/MWCNTs/Fe₃O₄-SH/Au in 0.1 M PBS and 0.1 mM BPA at different scan rates: (a) 0.025, (b) 0.050, (c) 0.075, (d) 0.10, (e) 0.15, (f) 0.20, (g) 0.25 and (h) 0.30 V s⁻¹. (A) Variation of the peak currents, I_p , vs. the scan rate, v . (B) Tafel plot recorded at scan rate 0.075 V s⁻¹. (C) Plot of the peak potentials versus log of scan rates.

obtained for electro-oxidation of BPA at the surface of nanocomposite. Also, the adsorbed amount of BPA on the GCE/MWCNTs/Fe₃O₄-SH/Au was calculated according to the following equation [34]:

$$I_p = nFQv/4RT = n^2F^2A\Gamma v/4RT \quad (2)$$

where n is the number of electron transferred, F (C mol⁻¹) is the Faraday's constant, A (cm²) is the area of the electrode, Γ is the surface coverage of adsorbed substance (mol cm⁻²), Q (C) is the quantity of charge consumed during the electro-oxidation reaction and v (V s⁻¹) is the scan rate. Based on the relationship of I_p with v and by integrating the peak area for BPA oxidation, the values of n and Γ_T were 2 and 1.40×10^{-10} mol cm⁻².

Based on Laviron theory for the irreversible voltammograms, peak potential (E_p) and scan rate v have relationship with following equation [35]:

$$E_p = E^0 - \frac{2.303RT}{anF} \log v + \frac{2.303RT}{anF} \log \frac{RTk_s}{anF} \quad (3)$$

where a is the transfer coefficient, k_s is the standard heterogeneous rate constant of the reaction, n is the number of electrons transferred, v is the scan rate and E^0 is the formal

redox potential and other symbols have their usual meanings. According to Figure 4(C), the oxidation peak potential was linear to the logarithm of scan rate with the regression equation as $E_p(V) = 0.0699 \log v (V s^{-1}) + 0.5910$ ($R^2 = 0.9886$). The value of an and k_s can be calculated to be 0.86 and $1.58 \times 10^{-10} s^{-1}$ for BPA. According to calculated charge transfer coefficient (Figure 4(B)), $\alpha = 0.43$, it can be concluded that two electrons are involved in the electro-oxidation of BPA at the surface of nanocomposite.

3.4 Study on pH of solution

Figure 5 shows the electrochemical response of nanocomposite on the determination of BPA in the various pH ranges from 5.0 to 10.0. From inset of Figure 5, it is seen that a linear reduction in the oxidation peak potential of BPA with slope value of 55.7 mV pH^{-1} was plotted as $E_p(V) = 0.9855 - 0.0557 \text{ pH}$ ($R^2 = 0.9952$). The slope value was close to the theoretically expected value of 59.0 mV pH^{-1} . The results showed the same number of proton and electron transmitted in the electrochemical reaction. Moreover, the peak currents of BPA also changed with pH values of the solution and the maximum anodic peak current was obtained at pH 9.0 (inset of Figure 5). The oxidation peak current increased with the growth of the pH when the pH values of buffer solution was lower than 9.0, but it decreased significantly when the pH of the solution was greater than 9.0, and so, pH 9.0 PBS was selected as the optimum pH for BPA detection.

3.5 Analytical performance

A review in various papers reveals that very few articles have been reported by amperometric method for determination of BPA. Figure 6 shows the steady-state amperometric current–time ($i-t$) curve of the GCE/MWCNTs/Fe₃O₄-SH/Au electrode in 0.1 M PBS for the successive addition of BPA at an applied potential 0.55 V. As illustrated from Figure 6, the proposed sensor shows a

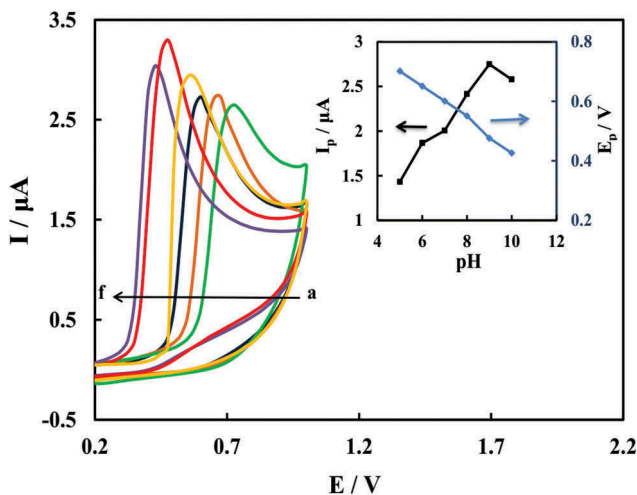


Figure 5. Cyclic voltammograms of GCE/MWCNTs/Fe₃O₄-SH/Au in 0.1 M PBS and 0.1 mM BPA at different pH values (from a to f: 5.0, 6.0, 7.0, 8.0, 9.0, and 10.0). Inset: variation of the peak currents versus pH and peak potentials versus pH.

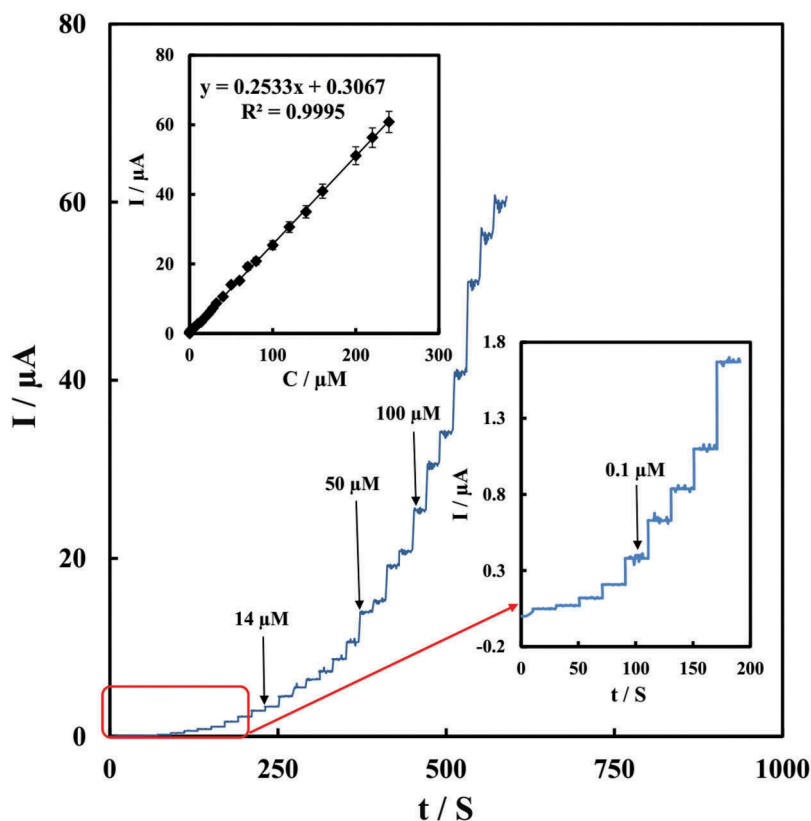


Figure 6. Amperometric response of the GCE/MWCNTs/Fe₃O₄-SH/Au in 0.1 M PBS upon successive additions of BPA. Inset: linear dependence of the peak currents with BPA concentration.

well-defined stepwise amperometric response current after the addition of BPA. The current reached the steady state in less than 5 s, indicating fast and highly sensitive current response of the GCE/MWCNTs/Fe₃O₄-SH/Au sensor to BPA reduction. As illustrated in inset of Figure 6, the sensor showed a linear response ranging from 0.002 μM to 240 μM and a detection limit of 6.73×10^{-10} M BPA (S/N = 3). Table 1 compares the performance of various modifiers for detection of BPA. Compared to the other reported BPA sensors (especially AuNPs-based sensors), the electrochemical parameters of BPA sensor in this present work are acceptable. The excellent performance of sensor likely results from exceptional conductivity of AuNPs and their synergistic effect with MWCNTs and Fe₃O₄ NPs.

3.6 Interference test and stability evaluation

The influence of various coexistent interference substances on the detection of BPA was investigated by amperometric method under optimised conditions. Interference study was done on some foreign species which may exist in biological samples such as glucose, fructose, lactose, sucrose, uric acid and some ions like Ca²⁺, Mg²⁺, NO₂⁻, Al³⁺, Co²⁺, Fe²⁺, Fe³⁺, K⁺, Na⁺, Cl⁻, SO₄²⁻, and NO₃⁻. Figure 7 shows current–time data of GCE/MWCNTs/Fe₃O₄-SH/Au for selective BPA detection, with interfering

Table 1. Comparison between various electroanalytical methods for determination of BPA with the proposed method.

Modifier	LOD (nM)	LDR (μM)	Method	pH	F_T (mol cm^{-2})	Ref.
Fe_3O_4 NPs- $\text{Si}_4\text{Pic}^+\text{Cl}^-/\text{Au}$	7.0	0.2–1.4	DPV	9.0	–	[4]
MWCNTs-COOH	3.5	0.004–0.105	FIA	7.0	–	[8]
NPs- $\text{Si}_4\text{Pic}^+\text{Cl}^-/\text{ELDH}^e$	6.8	0.02–1.51	DPV	8.5	2.55×10^{-11}	[16]
MIPPy ^f /GQDs ^d	40.0	0.1–50.0	DPV	7.0	–	[17]
PEI-PC ^g /DPNs ^h /AuNPs	6.63	0.01–300	Amperometry	7.4	–	[37]
Salicylaldehyde-modified chitosan	20	0.04–10	LSV	<1	7.32×10^{-11}	[38]
PHD ^f /MWCNTs	10	0.2–100	Amperometry	7	9.78×10^{-11}	[39]
CTS/MnO ₂ /CILE ^g	32	0.8–800	DPV	8	–	[40]
MWCNTs/Fe ₃ O ₄ -SH/Au	0.67	0.002–240	Amperometry	9.0	1.40×10^{-10}	This work

^gPolyethyleneimine-phosphatidylcholine.

^hDendritic platinum nanoparticles.

^fMolecularly imprinted polypyrrole.

^dGraphene quantum dots.

^eExfoliated Ni₂Al layered double hydroxide.

^fBlock polyelectrolyte composite films, composed of diblock polyelectrolyte poly (2-hydroxyethyl methacrylate)-b-poly (2-(dimethylamino) ethyl methacrylate) (PHEMA-bPDMAEMA, noted as PHD in the later content).

^gA carbon ionic liquid electrode (CILE) was fabricated by using ionic liquid N-hexylpyridinium hexafluorophosphate as the binder and the modifier. Then urchin-like MnO₂ microsphere and chitosan (CTS) was further casted on the CILE surface step-by-step to get a modified electrode that was denoted as CTS/MnO₂/CILE.

species added sequentially to the experimental solution, at time instants indicated by arrows in the figure. As shown in Figure 7, the first two signals of the graph are related to the BPA addition. No appreciable responses were observed for the excessive addition of interferences into the PBS (0.1 M, pH 9.0). The modified electrode revealed fast response time (response time is 1.5 s) and good selectivity to BPA molecules, which is more helpful for real sample analysis.

Reproducibility investigation of the sensor was studied by analysing BPA solutions of the same concentration at the surface of five similarly prepared modified electrodes and the RSD was calculated to be 4.7%. This result confirmed good reproducibility of the GCE/MWCNTs/

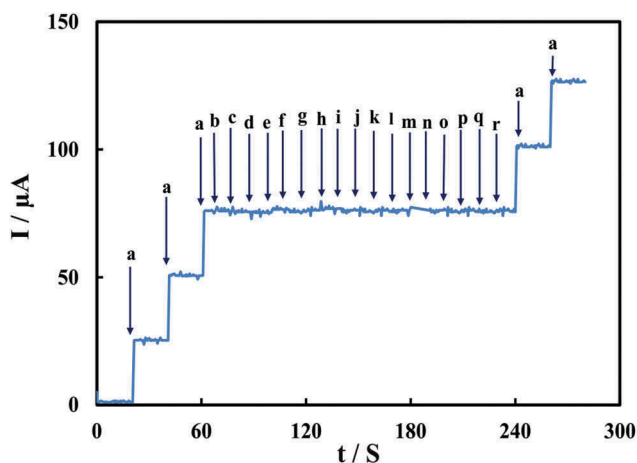


Figure 7. Amperometric response of the GCE/MWCNTs/Fe₃O₄-SH/Au in 0.1 M PBS upon successive additions of 100 μM BPA (a), 50 mM of each of glucose (b), fructose (c), lactose (d), urea (e), sucrose (f), NO_2^- (g), NO_3^- (h), SO_4^{2-} (i), Cl^- (j), Mg^{2+} (k), Ca^{2+} (l), Na^+ (m), K^+ (n) and 10 mM of each of Al^{3+} (o), Co^{2+} (p), Fe^{3+} (q) and Fe^{2+} (r). Applied potential is +0.55 V.

Fe₃O₄-SH/Au in the determination of BPA. The repeatability of proposed sensor was studied by evaluating the oxidation current of BPA on MWCNTs/Fe₃O₄-SH/Au. The relative standard deviation of the electrode response was only 4.3%, representing a proper repeatability. Since the fabricated sensor can be used for monitoring various real samples, evaluation of its long-term stability is an important aspect. The stability of the sensor was investigated by DPV technique using 100 µM BPA solution. After 2 months' storage at room temperature, the current response of electrode to 100 µM BPA decreased to 4.4% of its initial oxidation current. The exceptional long-term storage stability could be attributed to the high stability of synthesised nanocomposite on the electrode surface in the studied solution.

3.7 Real sample analysis

In a challenge to evaluate the possibility of the GCE/MWCNTs/Fe₃O₄-SH/Au for routine analysis, the sensor was applied to the analysis of different amount of spiked BPA in mineral water, milk and juice samples. After adjustment of the pH at optimum amount, the mineral water samples were tested without any further treatment. In the case of apple juice, precipitable materials were collected and separated from the medium by centrifugation at 4000 rpm for 5 min. The supernatant solution was diluted with 0.1 M PBS (pH 9.0) and used for electrochemical detection of BPA. Also, after adding 4.0 mL acetic acid (3%, v/v) to 4.0 mL liquid milk and standing for 15 min, it was diluted to 20.0 mL with deionised water. Then it was centrifuged for 10 min at 4000 rpm and the supernatant was collected. The sensor responses to BPA were compared with the values obtained by the spectrophotometric method [36]. Results are summarised in Table 2. Comparison of the results comprised in Table 2 shows good agreement of mentioned methods, thus reflecting the efficacy of the developed method for determination of BPA.

4. Conclusions

In this work, MWCNTs/Fe₃O₄-SH/Au nanocomposite was synthesised, characterised and used for modification of the surface of GCE. The resulting GCE/MWCNTs/Fe₃O₄-SH/Au showed good catalytic activity towards electro-oxidation of BPA. Initial investigations by cyclic voltammetry method showed that the oxidation peak current of BPA increased

Table 2. Determination results of BPA in real samples ($n = 5$).

Sample	Added (µM)	Found (µM)	RSD	Recovery (%)	Determined by spectrophotometry	RSD
Mineral water	0	–	–	–	–	–
	0.5	0.48 ± 0.01	2.1	95.6	0.51 ± 0.02	3.9
	5	4.98 ± 0.03	0.6	99.6	4.63 ± 0.04	0.9
Milk	0	–	–	–	–	–
	0.5	0.48 ± 0.02	3.6	95.2	0.49 ± 0.01	2.0
	5	5.4 ± 0.03	0.5	108.0	5.20 ± 0.05	1.0
Apple juice	0	–	–	–	–	–
	0.5	0.52 ± 0.01	1.9	104.1	0.50 ± 0.02	5.0
	5	4.77 ± 0.02	0.4	95.4	5.10 ± 0.02	0.4

Mineral water sample (Extra, Govaranoush Co., Khorasan, Iran).

Milk sample (Pegah, Iran Dairy Industries Co., Guilan, Iran).

Apple juice sample (Sun Star, Zarin Jam Marina Co., Tehran, Iran).

significantly with the decrease of the overpotential, which showed that the electron transfer rate of BPA was greatly enhanced on the surface of electrode. The amperometric responses showed that BPA can be sensed in the concentration range from 0.002 to 240 μM with the detection limit as 6.73×10^{-10} M. The proposed electrode showed good selectivity, reproducibility and stability, which provided its potential application as electrochemical sensor for detection of BPA for real samples.

Acknowledgments

We would like to thank the post-graduate office of Guilan University and Hakim Sabzevari University for the support of this work.

Disclosure statement

No potential conflict of interest was reported by the authors.

ORCID

Mehdi Baghayeri  <http://orcid.org/0000-0003-3004-1324>

References

- [1] An analysis of European plastics production, demand and waste data. <http://www.plasticseurope.org/Document/plastics-the-facts/>, 2014.
- [2] Y.-T. Wu, Y.-H. Zhang, M. Zhang, F. Liu, Y.-C. Wan, Z. Huang, L. Ye, Q. Zhou, Y. Shi and B. Lu, *Food Chem.* **164**, 527 (2014). doi:10.1016/j.foodchem.2014.05.071.
- [3] W.-Y. Chen, L.-P. Mei, -J.-J. Feng, T. Yuan, A.-J. Wang and H. Yu, *Microchim. Acta* **182**, 703 (2015). doi:10.1007/s00604-014-1377-4.
- [4] E.R. Santana, C.A. De Lima, J.V. Piovesan and A. Spinelli, *Sens. Actuators B* **240**, 487 (2017). doi:10.1016/j.snb.2016.09.003.
- [5] B. Nikahd and M.A. Khalilzadeh, *J. Mol. Liq.* **215**, 253 (2016). doi:10.1016/j.molliq.2015.12.003.
- [6] X. Xin, S. Sun, H. Li, M. Wang and R. Jia, *Sens. Actuators B* **209**, 257 (2015). doi:10.1016/j.snb.2014.11.128.
- [7] M. Baghayeri, R. Ansari, M. Nodehi, I. Razavipanah and H. Veisi, *Microchim. Acta* **185**, 320 (2018). doi:10.1007/s00604-018-2838-y.
- [8] M.S. Cosio, A. Pellicanò, B. Brunetti and A. Fuenmayor, *Sens. Actuators B* **246**, 673 (2017). doi:10.1016/j.snb.2017.02.104.
- [9] M.N. Tzatzarakis, E. Vakonaki, M.P. Kavvalakis, M. Barmpas, E.N. Kokkinakis, K. Xenos and A. M. Tsatsakis, *Chemosphere* **118**, 336 (2015). doi:10.1016/j.chemosphere.2014.10.044.
- [10] M.J. Gómez, M. Mezcuca, M.J. Martinez, A.R. Fernández-Alba and A. Agüera, *Int. J. Environ. Anal. Chem.* **86**, 3 (2006). doi:10.1080/03067310500247983.
- [11] X. Zhang, D. Zhu, C. Huang, Y. Sun and Y.I. Lee, *Microchem. J.* **121**, 1 (2015). doi:10.1016/j.microc.2015.01.012.
- [12] X. Wang, Y. Wang, Y. Shan, M. Jiang and J. Li, *Int. J. Environ. Anal. Chem.* **96**, 1480 (2016). doi:10.1080/03067319.2016.1271879.
- [13] A.D. Batista and F.R.P. Rocha, *Int. J. Environ. Anal. Chem.* **93**, 1402 (2013). doi:10.1080/03067319.2013.791974.
- [14] X. Niu, W. Yang, G. Wang, J. Ren, H. Guo and J. Gao, *Electrochim. Acta* **98**, 167 (2013). doi:10.1016/j.electacta.2013.03.064.
- [15] H. Beitollahi and S. Tajik, *Environ Monit. Assess.* **187**, 257 (2015). doi:10.1007/s10661-015-4506-6.

- [16] T. Zhan, Y. Song, Z. Tana and W. Hou, *Sens. Actuators B* **238**, 962 (2017). doi:10.1016/j.snb.2016.07.151.
- [17] F. Tan, L. Cong, X. Li, Q. Zhao, H. Zhao and X. Quan, J. Chen. *Sens. Actuators B* **233**, 599 (2016). doi:10.1016/j.snb.2016.04.146.
- [18] B. Deiminiat, G.H. Rounaghi, M.H. Arbab-Zavar and I. Razavipanah, *Sens. Actuators B* **242**, 158 (2016). doi:10.1016/j.snb.2016.11.041.
- [19] Y. Zhang, Y. Cheng, Y. Zhou, B. Li, W. Gu, X. Shi and Y. Xian, *Talanta* **107**, 211 (2013). doi:10.1016/j.talanta.2013.01.012.
- [20] E. Karaoglu, A. Baykal, H. Deligöz, M. S. Enel, H. Sözeri and M.S. Toprak, *J. Alloys Compd.* **509**, 8460 (2011). doi:10.1016/j.jallcom.2011.06.002.
- [21] T.D. Mai, F. d'Orlyé, C. Ménager, A. Varenne and J.M. Siaugue, *Chem. Commun.* **49**, 5393 (2013). doi:10.1039/c3cc41513a.
- [22] R. Gao, X. Mu, Y. Hao, L. Zhang, J. Zhang and Y. Tang, *J. Mater. Chem.* **2**, 1733 (2014). doi:10.1039/C3TB21684E.
- [23] E. Ebrahimpour, A. Amiri, M. Baghayeri, M. Rouhi and M.M. Lakouraj, *Microchem. J.* **131**, 174 (2017). doi:10.1016/j.microc.2016.12.022.
- [24] M. Rouhi, M. Mansour Lakouraj, M. Baghayeri and V. Hasantabar, *Int. J. Polymer. Mater.* **66**, 12 (2017). doi:10.1080/00914037.2016.1180615.
- [25] M. Baghayeri, E.N. Zare and M.M. Lakouraj, *Biosens. Bioelectron.* **55**, 259 (2014). doi:10.1016/j.bios.2013.12.033.
- [26] M. Baghayeri, E.N. Zare and M. Mansour Lakouraj, *Sens. Actuators B* **202**, 1200 (2014). doi:10.1016/j.snb.2014.06.019.
- [27] M. Najafi, M.A. Khalilzadeh and H. Karimi-Maleh, *Food Chemistry* **158**, 125 (2014). doi:10.1016/j.foodchem.2014.02.082.
- [28] H.-P. Peng, R.-P. Liang, L. Zhang and J.-D. Qiu, *J. Electroanal. Chem.* **700**, 70 (2013). doi:10.1016/j.jelechem.2013.04.016.
- [29] Q. Han, X. Shen, W. Zhu, C. Zhu, X. Zhou and H. Jiang, *Biosens. Bioelectron.* **79**, 180 (2016). doi:10.1016/j.bios.2015.12.017.
- [30] A.L. Andrade, D.M. Souza, M.C. Pereira, J.D. Fabris and R.Z. Domingues, *Cerâmica* **55**, 420 (2009). doi:10.1590/S0366-69132009000400013.
- [31] P. Abdul Rasheed, T. Radhakrishnan, P.K. Shihabudeen and N. Sandhyarani, *Biosens. Bioelectron.* **83**, 361 (2016). doi:10.1016/j.bios.2016.04.057.
- [32] M. Arvand, T.M. Gholizadeh and M.A. Zanjanchi, *Mater. Sci. Eng. C* **32**, 1682 (2012). doi:10.1016/j.msec.2012.04.066.
- [33] H. Yoo, M. Min, S. Bak, Y. Yoon and H. Lee, *J. Mater. Chem. A* **2**, 6663 (2014). doi:10.1039/C4TA00158C.
- [34] J. Wang, *Analytical Electrochemistry*, 3rd ed. (Wiley-VCH, Hoboken, New Jersey, 2000).
- [35] E. Laviron, *J. Electroanal. Chem.* **100**, 263 (1979). doi:10.1016/S0022-0728(79)80167-9.
- [36] N.K. Temel and R. Gürkan, *Anal. Methods* **9**, 1190 (2017). doi:10.1039/C6AY03064E.
- [37] K. Shim, J. Kim, M. Shahabuddin, Y. Yamauchi, S.A. Hossain and J.H. Kim, *Sens. Actuators B* **255**, 2800 (2018). doi:10.1016/j.snb.2017.09.096.
- [38] P. Deng, Z. Xu and Y. Feng, *Int. J. Environ. Anal. Chem.* **93**, 1116 (2013). doi:10.1080/03067319.2012.702276.
- [39] J. Yi, S. Tang, Z. Wang, Y. Yin, S. Yang, B. Zhang, S. Shu, T. Liu and L. Xu, *Int. J. Environ. Anal. Chem.* **95**, 158 (2015). doi:10.1080/03067319.2014.994616.
- [40] J. Lou, W. Wang, L. Yan, C. Ruan, X. Sun, W. Sun and P. Li, *Int. J. Environ. Anal. Chem.* **95**, 911 (2015). doi:10.1080/03067319.2015.1070407.